

7-2010

Mechanism Of N(5)-ethyl-flavinium Cation Formation Upon Electrochemical Oxidation Of N(5)-ethyl-4a-hydroxyflavin Pseudobase

Vincent Sichula

Ying Hu


Ekaterina Mirzakulova

Samuel F. Manzer

Shubham Vyas

See next page for additional authors

Follow this and additional works at: https://scholarworks.bgsu.edu/chem_pub

 Part of the [Chemistry Commons](#)

Repository Citation

Sichula, Vincent; Hu, Ying; Mirzakulova, Ekaterina; Manzer, Samuel F.; Vyas, Shubham; Hadad, Christopher M.; and Glusac, Ksenija D., "Mechanism Of N(5)-ethyl-flavinium Cation Formation Upon Electrochemical Oxidation Of N(5)-ethyl-4a-hydroxyflavin Pseudobase" (2010). *Chemistry Faculty Publications*. 131.
https://scholarworks.bgsu.edu/chem_pub/131

This Article is brought to you for free and open access by the Chemistry at ScholarWorks@BGSU. It has been accepted for inclusion in Chemistry Faculty Publications by an authorized administrator of ScholarWorks@BGSU.

Author(s)

Vincent Sichula, Ying Hu, Ekaterina Mirzakulova, Samuel F. Manzer, Shubham Vyas, Christopher M. Hadad, and Ksenija D. Glusac

Mechanism of N(5)-Ethyl-flavinium Cation Formation Upon Electrochemical Oxidation of N(5)-Ethyl-4a-hydroxyflavin Pseudobase

Vincent Sichula,[†] Ying Hu,[†] Ekaterina Mirzakulova,[†] Samuel F. Manzer,[‡] Shubham Vyas,[‡] Christopher M. Hadad,[‡] and Ksenija D. Glusac^{*,†}

Department of Chemistry, Bowling Green State University, Bowling Green, Ohio 43403, and Department of Chemistry, The Ohio State University, 100 West 18th Avenue, Columbus, Ohio 43210

Received: May 15, 2010; Revised Manuscript Received: June 16, 2010

We investigated the oxidation behavior of 5-ethyl-4a-hydroxy-3-methyl-4a,5-dihydrolumiflavin (pseudobase Et-FIOH) in acetonitrile with the aim of determining if the two-electron oxidized Et-FIOH²⁺ undergoes a release of hydroxyl cation and the production of 5-ethyl-3methylflavinium cation (Et-FI⁺). The focus of this work is to investigate the possibility of using Et-FIOH as a catalyst for water oxidation. The cyclic voltammetry demonstrates that Et-FIOH exhibits two one-electron oxidation potentials at +0.95 and +1.4 V versus normal hydrogen electrode (NHE), with the second oxidation potential being irreversible. The production of Et-FI⁺ is observed in the cyclic voltammetry of Et-FIOH and has been previously assigned to the release of OH⁺ from the two-electron oxidized Et-FIOH²⁺. The results of our study show that this is not the case: (i) we performed bulk electrolysis of the electrolyte solution at +2 V and then added Et-FIOH to the electrolyzed solution. We found that Et-FI⁺ is produced from this solution, even though Et-FIOH itself was not oxidized; (ii) reactions of Et-FIOH with chemical oxidants (ceric ammonium nitrate, nitrosyl tetrafluoroborate, and tetrabutylammonium persulfate) demonstrate that Et-FI⁺ production occurs only in the presence of strong Lewis acids, such as Ce⁴⁺ and NO⁺ ions. On the basis of these results, we propose that the production of Et-FI⁺ in the electrochemistry of Et-FIOH occurs because of the shift in the Et-FIOH/Et-FI⁺ acid–base equilibrium in the presence of protons released during anodic oxidation. We identified two sources of protons: (i) oxidation of traces of water present in the acetonitrile releases oxygen and protons and (ii) two-electron oxidized Et-FIOH²⁺ releases protons located on the N(5)-alkyl chain. The release of protons from Et-FIOH²⁺ was confirmed by cyclic voltammetry of Et-FIOH in the presence of pyridine as a base. The first oxidation peak of Et-FIOH at +0.95 V is reversible in the absence of pyridine. The addition of pyridine leads to the shift of the oxidation potential to a less positive value, which is consistent with a proton-coupled electron transfer (PCET). Furthermore, the anodic current increases, and the cathodic peak becomes irreversible, giving rise to two additional reduction peaks at –0.2 and –1 V. The same reduction peaks were observed in the high scan rate cyclic voltammogram of Et-FIOH in the absence of pyridine, implying that the release of protons indeed occurs from Et-FIOH²⁺. To determine which functional group of Et-FIOH⁺ is the source of protons, we performed DFT calculations at the B3LYP/6-311++G** level of theory for a reaction of Et-FIOH⁺ with pyridine and identified two proton sources: (i) the >N–CH₂– group of the N(5) alkyl chain and (ii) the –OH group in the 4a-position of the radical cation. Because the appearance of new reduction peaks at –0.2 and –1.0 V occurs in the model compound that lacks –OH protons (Et-FIOMe), we conclude that the proton removal occurs predominantly from the >N–CH₂– moiety.

Introduction

Flavin-dependent monooxygenases represent a class of flavoproteins that catalyze the incorporation of atomic oxygen into organic substrates.¹ The catalysis involves a reaction between molecular oxygen and the reduced flavin cofactor to produce a 4a-hydroperoxy derivative. The flavin moiety of the hydroperoxide derivative polarizes the O–O bond, which enables the release of atomic oxygen from the flavin to the organic substrate. A special class of monooxygenases is bacterial luciferases, which cause bioluminescence.² In the absence of the protein framework, the flavin cofactor reacts with oxygen to produce 4a-hydroperoxy derivative,³ but it does not act as a catalyst for insertion of atomic oxygen because of the fast release of

hydrogen peroxide. However, N(5)-ethyl flavinium perchlorate (Et-FI⁺, Figure 1) has been found to catalyze a range of oxidation reactions^{4–17} and has been used as a model system for mechanistic studies of bacterial luminescence.^{17–22}

Our interest in Et-FI⁺ was stimulated by previous reports suggesting that it may perform catalytic water oxidation. Two previously reported experiments suggested that such catalysis could occur: (i) Et-FI⁺ reacts with water to produce its pseudobase Et-FIOH²³ and (ii) two-electron electrochemical oxidation of Et-FIOH leads to the production of Et-FI⁺, possibly by releasing a hydroxyl cation.²⁰ The first reaction can be readily monitored by UV/vis absorption spectroscopy, as illustrated in Figure 1a. The pK_a value for the pseudobase formation is 3.6, which suggests that the reaction between Et-FI⁺ and hydroxide anion is thermodynamically favored ($\Delta G \approx -15$ kcal/mol). Figure 1b illustrates the second reaction. The cyclic voltammogram of Et-FI⁺ exhibits two reversible peaks at +0.17 and

* Corresponding author. E-mail: kglusac@bgsu.edu.

[†] Bowling Green State University.

[‡] The Ohio State University.

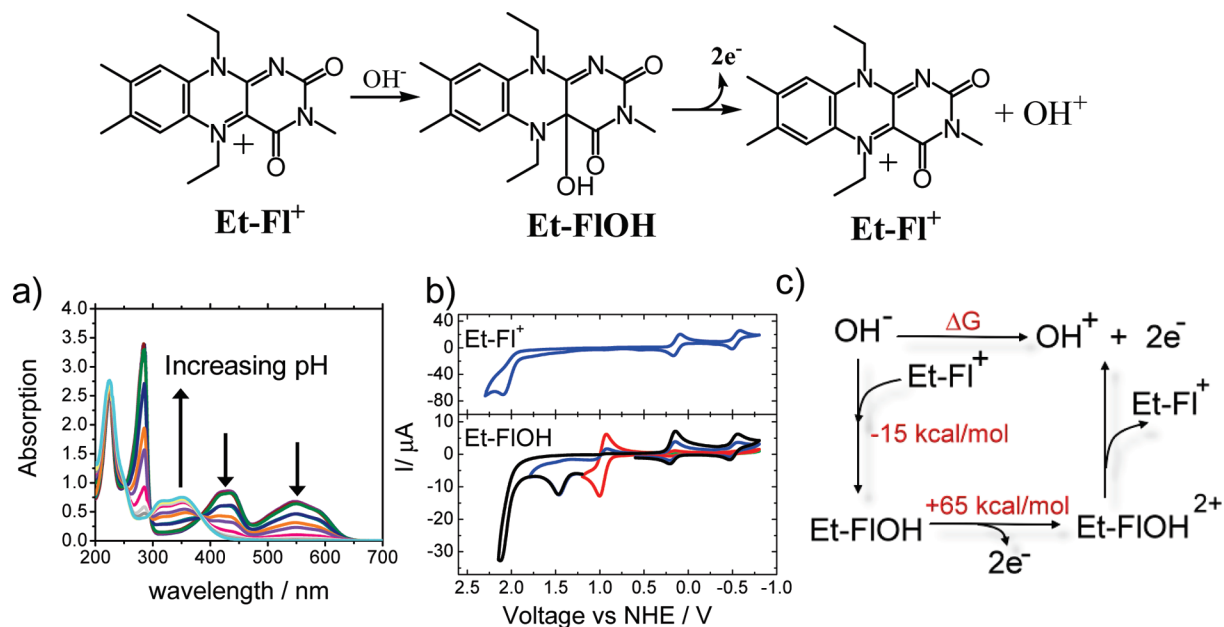


Figure 1. (a) pH-dependent absorption spectra of Et-FI⁺ in aqueous phosphate buffer (pH 0.7, 1.0, 2.0, 2.5, 3.0, 3.5, 4.0, 4.5, 5.0, 5.5, 5.7, 6.0, 6.5, and 7.0). (b) Cyclic voltammograms of Et-FI⁺ and Et-FIOH in acetonitrile (supporting electrolyte: 0.1 M Bu₄NClO₄, working electrode: platinum, scan rate: 0.1 V/s). (c) Thermodynamic cycle demonstrating the possibility of the OH⁺ release from Et-FIOH²⁺.

−0.52 V versus normal hydrogen electrode (NHE), which correspond to the reduction of Et-FI⁺ to produce semiquinone (Et-FI[•]) and hydroquinone (Et-FI[−]), respectively. The cyclic voltammogram of Et-FIOH consists of a reversible peak at $E_{1/2} = +0.95$ V due to one-electron oxidation of Et-FIOH and a second irreversible peak at $E = +1.4$ V that arises because of another one-electron oxidation to produce dication, Et-FIOH²⁺. When the voltage is scanned back to negative potentials, we observe a growth of peaks at +0.17 and −0.52 V that correspond to Et-FI⁺. These results suggest that the two-electron oxidation of Et-FIOH leads to the recovery of Et-FI⁺, possibly by creating a hydroxyl cation.²⁰ As shown in Figure 1c, the release of OH⁺ seems unlikely on the basis of thermodynamic considerations. We were unable to obtain the ΔG value for the two-electron oxidation of OH[−] to produce OH⁺. However, on the basis of thermodynamic parameters obtained from Figure 1a,b, the ΔG value needs to be less than or equal to +50 kcal/mol, which corresponds to the standard reduction potential of 1.1 V. The formation of OH⁺ at +1.1 V of potential seems highly unlikely. (For comparison, the standard reduction potential for $2\text{OH}^- \rightarrow \text{H}_2\text{O}_2 + 2\text{e}^-$ is 0.95 V.²⁴) However, even though the release of OH⁺ is unlikely, the release of molecular oxygen from Et-FIOH²⁺ is thermodynamically feasible (the standard reduction potential for reaction: $2\text{OH}^- \rightarrow \text{O}_2 + 2\text{H}^+ + 4\text{e}^-$ is only 0.815 V;²⁴ see the Supporting Information for a discussion of possible mechanism), which inspired us to investigate the process in more detail.

These previously published results suggest that Et-FI⁺ could be used to oxidize water catalytically, which would be an exciting avenue for the development of a fully organic water oxidation catalyst as an addition to the currently known organometallic catalysts.^{25–32} To investigate the oxidation behavior of Et-FIOH in more detail, we performed a series of electrochemical oxidation experiments on Et-FIOH and detailed supplementing density functional theory (DFT) calculations, which are presented in this article. These results suggest that the production of Et-FI⁺ from oxidized Et-FIOH²⁺ does not involve a release of an OH⁺ cation, but instead a shift in the Et-FIOH/Et-FI⁺ acid–base equilibrium due to the release of protons during the anodic oxidation of Et-FIOH.

Experimental Section

Syntheses. General Methods. All starting chemicals were purchased from Sigma-Aldrich chemicals and used as received. NMR spectra were recorded on a Bruker 300 MHz spectrometer. Electron impact ionization (EI) and MALDI mass spectra were measured on a Shimadzu QP5050A and a Bruker Daltonics Omnicflex mass spectrometer. For reactions that required an inert atmosphere, argon of standard quality was used.

4,5-Dimethyl-2-nitrofluoroacetanilide (2). Compound **2** was prepared according to the literature.³³ Trifluoroacetic acid anhydride (12.6 g, 60 mmol) was added dropwise to a stirred solution of **1** (4.98 g, 30 mmol) in methylene chloride (60 mL) cooled in ice bath. Triethylamine (9 mL) was added dropwise to the vigorously stirred solution. The reaction mixture was warmed to room temperature and stirred for 1 h. The reaction mixture was transferred to a separatory funnel and washed with 2 M HCl, NaHCO₃, and brine. The aqueous layer was extracted with dichloromethane. Combined organic extracts were dried over anhydrous sodium sulfate, filtered, evaporated, and dried over vacuum to give 7.58 g (96% yield) as a yellow solid. ¹H NMR (300 MHz, CDCl₃): 11.37 (s, 1H), 8.51 (s, 1H), 8.08 (s, 1H), 2.40 (s, 3H), 2.34 (s, 3H). EI-MS: m/z 262 (M⁺).

N-Ethyl-4,5-dimethyl-2-nitro-benzenamine (3). Compound **3** was prepared by the modified literature procedure.^{34,35} Compound **2** (6.55 g, 25 mmol) and K₂CO₃ (17.25 g, 125 mmol) were dissolved in 120 mL of DMF, and the reaction mixture was stirred for 30 min. Ethyl iodide (5.85 g, 37.5 mmol) was added dropwise and refluxed overnight. DMF was vacuum-evaporated, and the residue was dissolved in water and extracted with chloroform. The combined organic layers were dried with anhydrous Na₂SO₄, filtered, and concentrated in vacuum to yield a yellow-red residue. The residue was subjected to flash chromatography using dichloromethane as an eluent to give 4.51 g (93% yield) as an orange solid. ¹H NMR (300 MHz, CDCl₃): 7.93 (s, 1H), 7.80 (s, 1H), 6.62 (s, 1H), 3.33 (m, 2H), 2.27 (s, 3H), 2.18 (s, 3H), 1.36 (t, $J = 8$ Hz, 3H). ¹³C NMR (75 MHz, CDCl₃): 147.2, 144.2, 126.5, 124.2, 114.1, 37.7, 20.7, 18.5, 14.5. EI-MS: m/z 194 (M⁺).

N1-Ethyl-4,5-dimethyl-1,2-benzenediamine (4). Compound **3** (5.04 g, 26 mmol) was dissolved in 150 mL of concentrated HCl in a two-necked round-bottomed flask and purged with Ar. Excess tin foil (15.53 g, 131 mmol) was added to the reaction mixture and heated at 100 °C for 3 h under an inert atmosphere. The flask was cooled in an ice–water bath. Sodium hydroxide solution (~400 mL, 3.5 M) was added until the pH reached 10. This caused a white precipitation of SnO and the product. The reaction flask was heated to boil. The color of the precipitation changed to gray. The precipitate was filtered out and rinsed with 300 mL of boiling water. The filtrate was cooled in an ice–water bath to room temperature and extracted with chloroform and dried with anhydrous sodium sulfate under Ar. The solvent was evaporated to give the diamine **4**. Colorless crystals of **4** were obtained after drying under vacuum. 3.39 g (80% yield). ¹H NMR (300 MHz CDCl₃): 6.52 (s, 1H), 6.47 (s, 1H), 3.12 (q, *J* = 8 Hz, 2H), 2.12 (s, 3H), 2.13 (s, 3H), 1.28 (t, *J* = 8 Hz, 3H). EI-MS: *m/z* 164 (M⁺).

10-Ethyl-7,8-dimethyl-benzog[*g*]pteridine-2,4(3H,10H)-dione (5). Compound **5** was prepared according to a modified published procedure.³⁶ Diamine **4** (3.18 g, 20 mmol) was added to the solution of alloxane (6.4 g, 40 mmol) and boric acid (2.48 g, 40 mmol) dissolved in 100 mL of glacial acetic acid. The reaction mixture was stirred overnight under Ar at room temperature. Water (200 mL) was added to the reaction mixture and extracted with chloroform. The combined organic extracts were dried by sodium sulfate, filtered, and concentrated in a vacuum to yield a yellow residue. The residue was subjected to chromatography using CH₂Cl₂/MeOH (1:1) to give the pure compound 2.75 g (yield 51%). ¹H NMR (300 MHz, CDCl₃): 8.09 (s, 1H), 7.45 (s, 1H), 4.79 (q, *J* = 8 Hz, 2H), 2.58 (s, 3H), 2.47 (s, 3H), 1.50 (t, *J* = 8 Hz, 3H). MALDI MS: *m/z* 272 (MH₂⁺).

10-Ethyl-3,7,8-trimethyl-benzog[*g*]pteridine-2,4(3H,10H)-dione (6). Compound **6** was synthesized according to the literature.³⁵ K₂CO₃ (10.73 g, 78 mmol) was added to the suspended solution of **5** (2.10 g, 7.8 mmol) in 100 mL of DMF. Methyl iodide (11.08 g, 78 mmol, *V* = 4.9 mL) was added dropwise, and the reaction mixture was stirred at room temperature for 3 days. The progress of the reaction was monitored by TLC in an elute CH₂Cl₂/acetone 2:1 mixture. After the completion of the reaction, 200 mL of water was added. The aqueous solution was extracted with chloroform. The organic extracts were combined and dried with anhydrous sodium sulfate, filtered, and concentrated in vacuum to yield an orange product. The crude product was subjected to column chromatography using CH₂Cl₂/acetone 2:1 as an eluent to give 1.68 g of compound **6** (76% yield). ¹H NMR (300 MHz, CDCl₃): 8.09 (s, 1H), 7.43 (s, 1H), 4.78 (q, *J* = 8 Hz, 2H), 3.54 (s, 3H), 2.56 (s, 3H), 2.46 (s, 3H), 1.50 (t, *J* = 8 Hz, 3H). MALDI MS: *m/z* 285 (MH⁺).

5-Ethyl-3-methyl-1,5-dihydrolumiflavin (7). Synthesis of **7** was achieved using the published procedure.²³ Compound **6** (0.284 g, 1 mmol) was suspended in 10 mL of ethanol. The mixture was purged with nitrogen and cooled to 0 °C. Sodium hydroxide (10 mL, 1 M) and sodium dithionite (0.5 g, 35 mmol) were added to the reaction mixture. Ethyl iodide (1.2 g, *V* = 1.0 mL, 8 mmol) was added dropwise for 30 min. The reaction mixture was stirred overnight and then acidified with glacial acetic acid (pH 3 to 4). Ethanol was removed under reduced pressure, and an orange precipitate formed while the remaining watery phase was cooled. The precipitate was filtered, washed with dithionite-containing water, and dissolved in dithionite containing 5 M ammonia. The insoluble residue was filtered

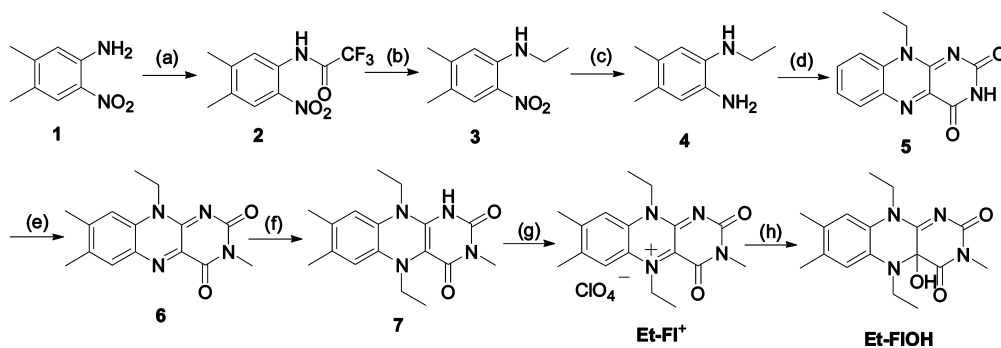
out, and the filtrate was acidified with glacial acetic acid. The resulting precipitate was collected, washed with dithionite-containing water, and dried under vacuum to give 0.270 g of orange compound (yield 85%). ¹H NMR (300 MHz, CDCl₃ overlaid with D₂O/Na₂S₂O₄): 6.68 (s, 1H), 6.44 (s, 1H), 3.75 (q, *J* = 8 Hz, 2H), 3.37 (q, *J* = 8 Hz, 2H), 3.28 (s, 3H), 2.14 (s, 3H), 2.10 (s, 3H), 1.28 (t, *J* = 8 Hz, 3H), 1.07 (t, *J* = 8 Hz, 3H).

5-Ethyl-3-methyl-lumiflavinium Perchlorate (Et-FI⁺). Et-FI⁺ was synthesized according to the published procedure.²³ Compound **7** (0.314 g, 1 mmol) was dissolved in 10 mL of dithionite containing ammonia and filtered. The filtrate was added to 15 mL of 70% HClO₄. Then, NaNO₂ (0.50 g, 7 mmol) and NaClO₄ (0.50 g, 4 mmol) were added to the reaction mixture. The reaction mixture was stirred at 10 °C for 2 h. The resulting purple precipitate was filtered and washed with water, MeOH, ether, and CHCl₃ to yield 0.264 g (yield 75%) of the product. ¹H NMR (CD₃CN, 300 MHz, δ): 1.00 (3H, t, *J* = 6.9 Hz, CH₂–CH₃), 1.25 (3H, t, *J* = 6.8 Hz, CH₂–CH₃), 2.30 (3H, s, –CH₃ arom.), 2.32 (3H, s, –CH₃ arom.), 3.21 (3H, s, N–CH₃), 3.43 (2H, q, *J* = 7 Hz, CH₂–CH₃), 4.25 (2H, q, *J* = 7.2 Hz, CH₂–CH₃), 7.09 (1H, s, C–H arom.), 7.20 (1H, s, C–H arom.). MALDI-MS: *m/z* 314 (M⁺).

5,10-Diethyl-4a,5-dihydro-4a-hydroxy-3,7,8-trimethylbenzog[*g*]pteridine-2,4(3H,10H)-dione (Et-FIOH). Et-FIOH was prepared according to published procedure.²³ Et-FI⁺ (200 mg) **8** was dissolved in 2 mL of water/acetonitrile mixture (1:10), and 10 mL of 0.1 M phosphate buffer at pH 7 was added to the solution. The mixture was stirred for 10 min, and the resulting light-yellow precipitate was filtered and crystallized from acetone/water. Et-FIOH was obtained in 63% yield (94 mg). ¹H NMR (300 MHz, CDCl₃): 7.06 (s, 2H), 4.37 (m, 2H), 3.40 (m, 5H), 2.91 (s, 1H), 2.31 (s, 3H), 1.27 (t, *J* = 8 Hz, 3H), 0.98 (t, *J* = 8 Hz, 3H). MALDI-MS: *m/z* 330 (M⁺).

5,10-Diethyl-4a,5-dihydro-4a-methoxy-3,7,8-trimethylbenzog[*g*]pteridine-2,4(3H,10H)-dione (Et-FIOMe). Et-FIOMe was synthesized according to published procedure.³⁷ Et-FI⁺ (0.11 g, 2.7 mmol) was dissolved in 3 mL of methanol, and sodium metal (0.014 g, 6.1 mmol) was added. The reaction mixture was stirred for 30 min at room temperature. The precipitate was filtered off and washed with methanol to give 62 mg (yield 67%) as a light-yellow solid. ¹H NMR (300 MHz, CD₃CN): 7.19 (s, 1H), 7.12 (s, 1H), 4.31 (m, *J* = 3 Hz, 2H), 3.58 (m, *J* = 7.2 Hz, 2H), 3.26 (s, 3H), 3.04 (s, 3H), 2.30 (s, 6H), 1.27 (t, *J* = 7.2 Hz, 3H), 1.08 (t, *J* = 6.9 Hz, 3H). MALDI: *m/e* 344 (M⁺).

Electrochemistry. All electrochemical measurements were done in acetonitrile using tetrabutyl-ammonium perchlorate (TBAP) as a supporting electrolyte. Acetonitrile was purchased from Sigma-Aldrich (Anhydrous, 99.8%). The solvent was refluxed over CaH₂ for 8 h and then distilled. Anhydrous pyridine was purchased from Sigma-Aldrich. Pyridine (20 mL) was left to stand overnight over 4 g of NaOH pellets. Pyridine was filtered off, refluxed over BaO for 4 h, and then distilled and stored over 4 Å molecular sieves. TBAP was purchased from Fluka, recrystallized from methanol, and dried under vacuum. Cyclic voltammetry and bulk electrolysis were done using an EC Epsilon potentiostat (Bioanalytical Systems). Cyclic voltammetry was performed in a VC-2 voltammetry cell (Bioanalytical Systems) using platinum working electrode (1.6 mm diameter, MF-2013, Bioanalytical Systems), platinum wire auxiliary electrode (MW-4130, Bioanalytical Systems), and nonaqueous Ag/Ag⁺ reference electrode (MF-2062, Bioanalytical Systems). Bulk electrolysis was performed in a cell (MF-1056, Bioanalytical Systems) equipped with reticulated vitreous

SCHEME 1: Synthetic Procedure for the Preparation of Et-FI⁺ and Et-FIOH^a

^a (a) $(\text{CF}_3\text{CO})_2\text{O}$, CH_2Cl_2 , Et_3N (96%); (b) EtI , K_2CO_3 , DMF , 100°C (93%); (c) HCl , Sn , 100°C (80%); (d) alloxane, H_3BO_3 , AcOH (51%); (e) MeI , K_2CO_3 , DMF (76%); (f) $\text{Na}_2\text{S}_2\text{O}_4$, EtI , EtFIOH , NaOH (85%); (g) $\text{Na}_2\text{S}_2\text{O}_4$, NH_4OH , HClO_4 , NaNO_2 , NaClO_4 , 10°C (75%); (h) CH_3CN , phosphate buffer at pH 7 (63%).

carbon electrode, coiled Pt wire auxiliary electrode within a fritted glass isolation chamber, and a Ag/AgCl reference electrode. Absorption spectra were recorded on Agilent 8453 UV spectrometer in a 2 mm quartz cell. UV/vis absorption spectroelectrochemistry was done using a gold-gauze working electrode and a cell/spectrometer system previously described.³⁸

Computational Methods. All calculations were performed at the Ohio Supercomputer Center using the Gaussian 03 software package.³⁹ Geometry optimizations were carried out at the B3LYP/6-31G* level of theory.^{40,41} We performed vibrational frequency analyses to verify that the optimized geometries were true energy minima with zero calculated imaginary frequencies. Further single-point energies for each optimized geometry were calculated at the B3LYP/6-311++G** level. Solvation calculations were carried out using the polarization continuum model (PCM)^{42–47} for acetonitrile, as implemented in Gaussian 03. Both spin densities and charge densities were obtained through natural population analysis (NPA) at the B3LYP/6-311++G** level of theory.

Reactions of Et-FIOH with Chemical Oxidants. Chemical oxidation was performed in acetonitrile using three oxidants: (i) ceric ammonium nitrate (CAN, 99.99%, Sigma-Aldrich), (ii) nitrosyl tetrafluoroborate (NO, 95%, Sigma-Aldrich), and (iii) TBAPS. The syntheses of TBAPS were achieved from tetrabutylammonium hydrogen sulfate (Sigma-Aldrich) and potassium persulfate (Acros Organics) according to the published procedure.⁴⁸ The changes in the UV/vis absorption spectra were monitored using Agilent 8453 UV spectrometer in a 2 mm cell. The concentration of Et-FIOH was 10^{-5} M in all experiments.

Results and Discussion

Syntheses. The flavinium salt Et-FI⁺ and its pseudobase Et-FIOH were synthesized according to Scheme 1. The first two reactions were conducted with a goal of converting 4,5-dimethyl-2-nitroaniline (**1**) to monoalkylated compound **3**. To avoid dialkylation of the amine, compound **1** was initially reacted with trifluoroacetic anhydride to produce amide **2**. Further alkylation of the amide **2** using ethyl iodide, followed by hydrolysis yielded monoalkylated compound **3** in excellent yield. A similar method was used previously to obtain a 2-methoxyethyl amino derivative.³⁴ The subsequent reduction of nitro-group using Sn/HCl afforded bis-amine **4**, which was found to be unstable in the presence of oxygen. To avoid large losses, compound **4** was immediately reacted with alloxane using a condensation method developed by Kuhn.³⁶ The N3 position of product **5** was methylated using methyl iodide to afford model compound **6**. The conversion of **6** to flavinium salt Et-FI⁺ was achieved in a

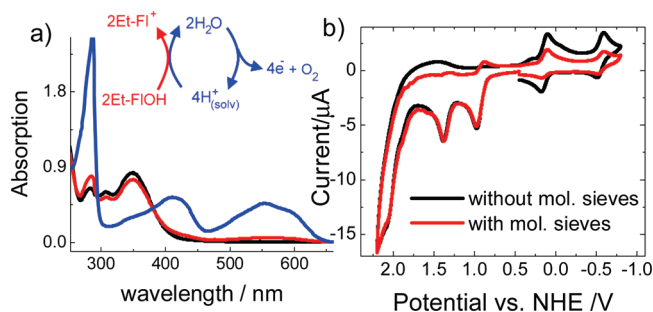


Figure 2. (a) Electrolyte solution (0.1 M TBAP in acetonitrile) was electrolyzed for 10 min at +2 V versus NHE; then, Et-FIOH was added to the solution. UV/vis absorption spectra were collected as follows: using freshly distilled acetonitrile (black); 0.5 h after distillation (red); 4 h after distillation (blue). (b) Cyclic voltammograms of Et-FIOH in acetonitrile containing 0.1 M TBAP (scan rate: 0.1 V/s): without 4 Å molecular sieves (black); with molecular sieves (red).

two-step reaction using a procedure developed by Müller.²³ In the initial step, **6** was reduced to its hydroquinone form **7** using sodium dithionite, then ethylated using ethyl iodide to form EtFIH. Compound EtFIH reacts with oxygen to produce 4a-hydroperoxy derivative Et-FIOOH.¹⁷ To avoid product losses due to this reaction, we kept the product under an inert atmosphere and immediately reacted in the next step, which involved the oxidation using NaNO_2 and HClO_4 to produce the final product Et-FI⁺. The formation of Et-FIOH pseudobase from Et-FI⁺ was achieved using acetonitrile/water mixture at pH 7.²³

Electrochemistry. We performed bulk electrolysis of the electrolyte solution (0.1 M TBAP in acetonitrile) at +2 V. After 10 min of electrolysis, we added a small amount of solid Et-FIOH to the solution and measured the UV/vis absorption spectrum. Figure 2a demonstrates the conversion of Et-FIOH (absorbs at 355 nm) to Et-FI⁺ (absorbs at 420 and 550 nm), even if Et-FIOH itself was not oxidized. The amount of produced Et-FI⁺ increases with the amount of water present in the electrolyte solution, which is evident from the spectra obtained at different time intervals after acetonitrile distillation. These results suggest that the oxidation of water at +2 V leads to a release of molecular oxygen and solvated protons. The solvated protons decrease the pH of the solution and lead to the production of Et-FI⁺. Further evidence of the water oxidation can be seen from Figure 2b, which shows the cyclic voltammograms of Et-FIOH in acetonitrile in the absence and presence of 4 Å molecular sieves. The amount of Et-FI⁺ produced is smaller in the presence of molecular sieves, as judged by the current intensities at +0.17 and -0.52 V (reduction peaks of

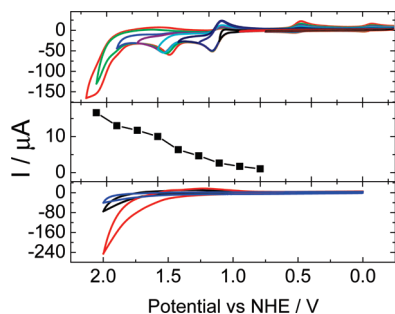


Figure 3. (a) Cyclic voltammograms of 3 mM Et-FIOH in acetonitrile (0.1 M TBAP) obtained at different switching potentials; sweep rate: 100 mV/s. (b) Plot of current at 0.09 V (Et-FI⁺ reduction peak) obtained during return scans (cyclic voltammograms in part a) as a function of switching potential. (c) Cyclic voltammograms of 0.1 M TBAP in freshly distilled acetonitrile (blue), nondistilled acetonitrile (black), and acetonitrile/water 9:1 mixture (red). Sweep rate: 100 mV/s.

Et-FI⁺). It is important to note that even small traces of water will cause a strong effect because the reaction of protons with Et-FIOH creates new equivalents of water that can repeat the cycle (inset scheme in Figure 2).

The pH decrease due to water oxidation could account for Et-FI⁺ formation in the electrochemical oxidation of Et-FIOH. Figure 3 represents the effect of switching potential on the electrochemical behavior of Et-FIOH. As the switching potential is increased, more current is observed in return scans at potentials for Et-FI⁺ at +0.17 and -0.52 V. Figure 3b shows the dependence of current at +0.09 V (Et-FI⁺ reduction peak) as a function of switching potential. It can be seen that Et-FI⁺ becomes produced once the switching potential exceeds the value of +1.2 V and increases for higher switching potentials. Figure 3c shows how the presence of water influences the cyclic voltammogram of 0.1 M TBAP in acetonitrile. We can see that water oxidation becomes significant at potentials above +1.2 V, the same potential at which Et-FI⁺ becomes produced, suggesting that the water oxidation mechanism can account for the production of Et-FI⁺ from Et-FIOH.

Another electrochemical process that could lead to a pH decrease is the oxidation of the electrolyte (TBAP). Perchlorate anion undergoes one-electron oxidation at +2.3 V,⁴⁹ and the produced perchlorate radicals are known to abstract hydrogen atoms from acetonitrile to produce perchloric acid.⁵⁰ To investigate the role of electrolyte, we obtained cyclic voltammograms of Et-FIOH at different concentrations of TBAP, and we plotted the resulting current at 0.09 V as a function of switching potential (Figure 4). The amount of Et-FI⁺ produced remained unaffected by TBAP concentrations, and thus the pH decrease in aforementioned experiments is not due to TBAP oxidation.

Reactions with Chemical Oxidants. Further confirmation that Et-FI⁺ is not produced as a result of the release of a hydroxyl cation from Et-FIOH²⁺ comes from the reactions of Et-FIOH with chemical oxidants (Figure 5). We investigated the reaction of Et-FIOH with three oxidants: (i) CAN, (ii) nitrosyl tetrafluoroborate (NOBF₄), and (iii) TBAPS. The progress of each reaction was monitored by UV/vis absorption spectroscopy (Figure 5). The production of Et-FI⁺ (absorbs at 420 and 550 nm) was observed in the presence of CAN and NOBF₄. The production of Et-FI⁺ in these cases is instantaneous and almost quantitative: In the presence of NOBF₄, Et-FIOH converts to Et-FI⁺ with ~100% efficiency. The effect of CAN on Et-FIOH is dual: it converts Et-FIOH to Et-FI⁺; then, it reacts with Et-FI⁺ (as confirmed by mixing Et-FI⁺ and CAN and monitoring

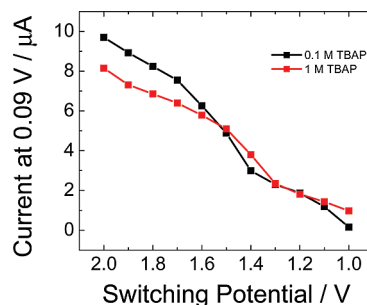


Figure 4. Cyclic voltammograms of Et-FIOH in acetonitrile were obtained as a function of switching potential. Sweep rate: 100 mV/s. The current at 0.09 V (peak due to Et-FI⁺) was plotted as a function of switching potential. Black curve represents data obtained using 0.1 M TBAP solution, whereas the red curve was obtained using 1 M TBAP solution.

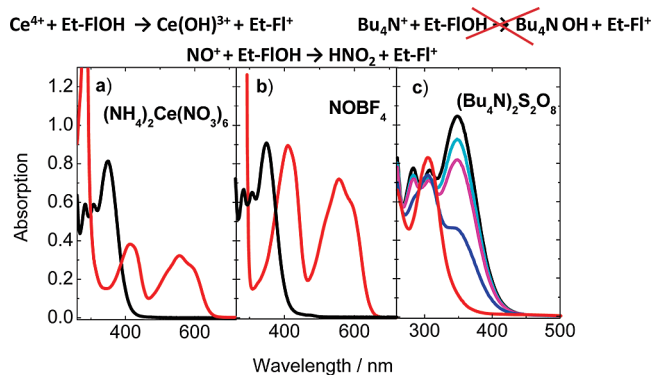


Figure 5. Black lines represent the absorption spectrum of Et-FIOH in acetonitrile. (a) Red line: the absorption spectrum obtained after the addition of 2 equiv of CAN. (b) Red line: the absorption spectrum obtained after the addition of 2 equiv of NOBF₄. (c) Two equiv of TBAPS was added to Et-FIOH solution at 40 °C. The spectra were obtained 10 (cyan), 20 (magenta), 30 (blue), and 40 (red) min after the addition.

the changes in the UV/vis absorption, data not shown). Therefore, the smaller yield of Et-FI⁺ produced in the reaction of CAN with Et-FIOH is explained by the decomposition of Et-FI⁺ in the presence of CAN. On the contrary, the production of Et-FI⁺ in the presence of persulfate ions was not observed. Instead, the oxidation leads to the slower increase in the oxidation product at 310 nm.

Table 1 lists the oxidation potentials of the compounds used in this study. The reported values for NOBF₄ and CAN were obtained in acetonitrile,^{51,52} whereas the reported potential for TBAPS was obtained in water.⁵³ The TBAPS potential might be different in acetonitrile, but it can be safely assumed that it remains higher than the two-electron potential of Et-FIOH. The potentials presented in Table 1 demonstrate that NOBF₄ and TBAPS can be used to achieve the two-electron oxidation of Et-FIOH, whereas CAN is not a strong enough oxidant in acetonitrile to produce Et-FIOH²⁺. Even though persulfate ion is the strongest oxidizing agent in Table 1, the production of Et-FI⁺ was not observed when Et-FIOH was treated with TBAPS. At the same time, the production of Et-FI⁺ was almost quantitative in the presence of NOBF₄, which barely has enough oxidizing power to perform a two-electron oxidation of Et-FIOH. Furthermore, the formation of Et-FI⁺ was observed in the presence of CAN, which cannot perform a two-electron oxidation of Et-FIOH. This result led us to conclude that the production of Et-FI⁺ is not associated with the oxidation of Et-FIOH. For example, the oxidation of Et-FIOH seems to occur only in the presence of TBAPS, and the oxidized product does

TABLE 1: Lewis Acidity and Standard Reduction Potentials of the Compounds Used

reaction	K_{eq}/M^{-1}	reaction	E°/V
$Et-FI^{+} + OH^{-} \rightarrow Et-FIOH$	$5.5 \times 10^{10}{}^a$	$Et-FIOH^{2+} + 2e^{-} \rightarrow Et-FIOH$	$\sim +1.4{}^c$
$Ce^{4+} + OH^{-} \rightarrow Ce(OH)^{3+}$	$5.2 \times 10^{14}{}^b$	$Ce^{4+} + e^{-} \rightarrow Ce^{3+}$	$+0.75{}^{51}$
$NO^{+} + OH^{-} \rightarrow HNO_2$	$3.3 \times 10^{20}{}^b$	$NO^{+} + e^{-} \rightarrow NO$	$+1.527{}^{52}$
$Bu_4N^{+} + OH^{-} \rightarrow Bu_4NOH$	$1 \times 10^5{}^{67}$	$SO_4^{-} + e^{-} \rightarrow SO_4^{2-}$	$+2.43{}^{53}$

^a Equilibrium constant was obtained from pH-dependent UV/vis spectra presented in Figure 1a. ^b Equilibrium constants were calculated using the constants reported for reactions of given cations with water: $Ce^{4+} + H_2O \rightarrow Ce(OH)^{3+} + H^{+}$ ($K = 5.2$)⁶⁸ and $NO^{+} + H_2O \rightarrow 2H^{+} + NO_2^{-}$ ($K = 0.33 \times 10^7$).⁶⁹ These constants were divided by water dissociation constant ($K = 1 \times 10^{-14}$) to provide constants reported in Table 1. ^c An estimate of the standard reduction potential obtained from the cyclic voltammogram of Et-FIOH presented in Figure 1b. ^d Experiments were conducted at 40 °C, a temperature at which $S_2O_8^{2-}$ decomposes into two sulfate radical anions.⁷⁰

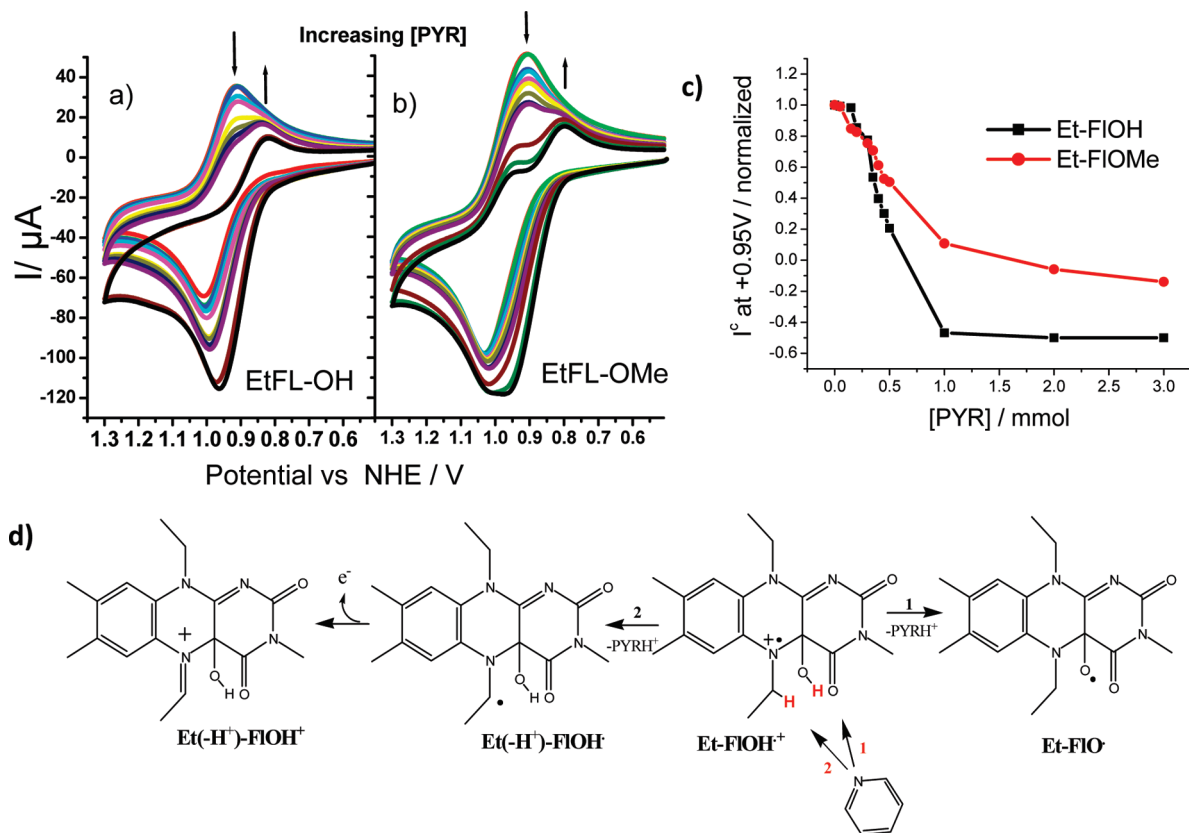


Figure 6. Cyclic voltammograms of (a) Et-FIOH and (b) Et-FIOMe in acetonitrile with increasing concentration of pyridine. Pyridine concentrations varied from 0 to 3 mM. Electrolyte: 0.1 M TBAP. Sweep rate: 150 mV/s. (c) Plot of normalized cathodic current at +0.95 V for Et-FIOH (black) and Et-FIOMe (red) as a function of pyridine concentration. (d) Scheme illustrating possible deprotonation sites in Et-FIOH⁺.

not exhibit any absorption at 420 and 550 nm, where Et-FI⁺ absorbs. This result suggests that the oxidation of Et-FIOH leads to the product that absorbs at 310 nm. Instead, Et-FI⁺ production was observed only in the presence of strong Lewis acids Ce⁴⁺ and NO⁺, suggesting that the reaction involves a transfer of OH⁻ from Et-FIOH to ceric and nitrosyl cations. Table 1 lists the equilibrium constants for reaction of cations involved in this study with OH⁻ ions. Even though the reported acid/base constants were measured in water, it is safe to assume a linear dependence of the equilibrium constants going from water to acetonitrile [$pK_a(CH_3CN) = 5.2 + 1.313pK_a(H_2O)$].⁵⁴ From these data, we can see that the transfer of OH⁻ from Et-FIOH to Ce⁴⁺ or NO⁺ is a thermodynamically favored process, whereas the transfer of OH⁻ from Et-FIOH to Bu₄N⁺ is not. These calculations fully support the mechanism in which the Et-FI⁺ formation is associated with a Lewis-type acid–base reaction between Et-FIOH and Lewis acids Ce⁴⁺ and NO⁺.

Effect of Pyridine. The data presented so far demonstrate that the formation of Et-FI⁺ occurs because of the reaction of Et-FIOH with Bronsted or Lewis acids present in the solution. We demonstrated that the anodic oxidation of water decreases the solution pH, leading to the production of Et-FI⁺ from Et-FIOH. However, these results do not address the role of two-electron oxidized Et-FIOH²⁺ in Et-FI⁺ formation. We postulated that Et-FIOH²⁺ could also contribute to the decrease in the solution pH by a reaction: $Et-FIOH^{2+} \rightarrow Et-FIOH^{+} + H^{+}$. To investigate this possibility, we analyzed the electrochemical oxidation of Et-FIOH in the presence of pyridine as a base. As can be seen from Figure 6a, the reversible one-electron oxidation potential of Et-FIOH shifts slightly to the less positive value as the pyridine concentration is increased. We interpret this result in terms of proton-coupled electron transfer (PCET):^{55–57} One-electron oxidation of Et-FIOH leads to the formation of radical cation, Et-FIOH⁺. Because of its positive charge, Et-FIOH⁺

is acidic, and it loses a proton in the presence of pyridine to produce $\text{Et}(-\text{H}^+)-\text{FIOH}\cdot$ radical (Figure 6c). PCET generally occurs by either coupled CEP process (electron and proton are transferred in a single step) or consecutive ET/PT or PT/ET process. On the basis of the fact that the initial anodic peak of Et-FIOH does not shift significantly to the lower potential (Figure 6a), we postulate that the consecutive ET/PT mechanism takes place. The consecutive ET/PT process is also consistent with the thermodynamic cycle presented in Figure S3 of the Supporting Information. Previous pulse radiolysis experiments suggest that the loss of proton occurs upon one-electron oxidation of Et-FIOH.⁵⁸ The $\text{p}K_{\text{a}}$ value of $\text{Et-FIOH}^{+\cdot}$ was estimated to be 3.7, whereas the $\text{p}K_{\text{a}}$ value of Et-FIOH is ~ 10 . The change in the $\text{p}K_{\text{a}}$ value upon oxidation is rather modest in comparison with systems in which the coupled CEP process occurs. (For example, $\text{p}K_{\text{a}}$ value of dihydroanthracene drops from +41 to -15 upon oxidation.)⁵⁹ Using this value, we estimated the ΔG values for coupled CEP and consecutive ET/PT processes (Figure S3). The results show that $\Delta G^{\text{ET}} < \Delta G^{\text{CEP}}$. Assuming that the activation barriers depend linearly on ΔG , we can conclude that the consecutive mechanism is more likely to occur. The proton is most probably removed from the $-\text{CH}_2$ moiety of the N(5)-ethyl group, as will be discussed in the following paragraph. In addition to the shift of the oxidation potential, we observed an increase in the anodic current at increasing pyridine concentrations. We assign this increase to an additional one-electron oxidation following initial PCET, which converts the neutral $\text{Et}(-\text{H}^+)\text{FIOH}\cdot$ radical to $\text{Et}(-\text{H}^+)\text{FIOH}^+$ iminium ion (Figure 6c). Additional oxidation frequently accompanies initial PCET processes^{60–62} because charge neutralization achieved by proton removal facilitates the elimination of the second electron from neutral radical, in our case $\text{Et}(-\text{H}^+)\text{FIO}\cdot$. Therefore, the second oxidation peak of Et-FIOH moves from $\sim +1.4$ V in the absence of pyridine to $\sim +0.95$ V in the presence of base, and the overall oxidation process that occurs at $+0.95$ V in the presence of pyridine involves a net transfer of two electrons and a proton, producing an iminium ion, $\text{Et}(-\text{H}^+)\text{FIOH}^+$, as illustrated in Figure 6c.

The remaining question is which proton is being removed from $\text{Et-FIOH}^{+\cdot}$ radical cation. In the case of neutral Et-FIOH, the most acidic proton is located on the $-\text{OH}$ group, with a $\text{p}K_{\text{a}}$ value of 9.2.¹⁰ Upon formation of $\text{Et-FIOH}^{+\cdot}$, it is reasonable to expect a $\text{p}K_{\text{a}}$ shift to a value lower than 9.2 and that the deprotonation would lead to the formation of $\text{Et-FIO}\cdot$ radical. To determine if this is the case, we prepared 4a-methoxyflavin derivative (Et-FIOMe) and investigated its oxidation behavior in the presence of pyridine. Because Et-FIOMe lacks acidic O–H proton, we anticipated that the oxidation behavior of Et-FIOMe would remain unaffected by the presence of pyridine. To our surprise, we found that this is not the case. Figure 6b demonstrates that Et-FIOMe undergoes qualitatively the same PCET process as Et-FIOH, suggesting that the proton is not being removed the $-\text{OH}$ moiety. Because both Et-FIOH and Et-FIOMe undergo a similar reaction with pyridine, we propose that the source of protons is not the $-\text{OH}$ moiety but instead the N(5)-ethyl group. It is well known that amine radical ions are acidic and that they lose protons from α -carbons.^{63,64} In the case of $\text{Et-FIOH}^{+\cdot}$, the positive charge is mostly localized on the N(5)-atom, making the protons located on neighboring $-\text{CH}_2-$ group the most probable candidates for deprotonation. This conclusion is further supported by previous studies on Et-FI^+ chemistry,¹⁷ showing that Et-FI^+ undergoes base-catalyzed decomposition to lumiflavin, the process being initiated by a loss of proton from the N(5)- CH_2- group.

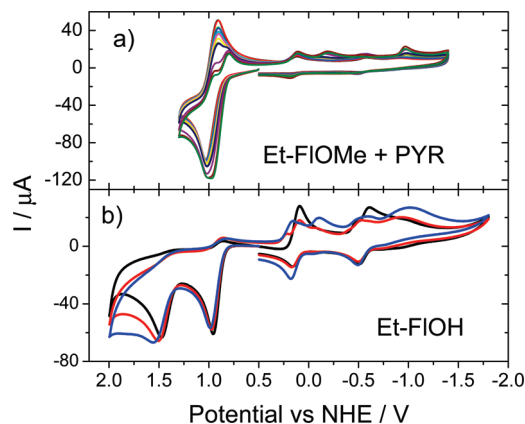


Figure 7. (a) Cyclic voltammograms of Et-FIOMe in acetonitrile in the presence of varying concentrations of pyridine (0–3 mM). Supporting electrolyte: TBAP; sweep rate: 0.1 V/s. (b) Variable scan rate, background-subtracted cyclic voltammograms of Et-FIOH in 0.1 M TBAP. Sweep rates: 1 (black), 5 (red), and 10 V/s (blue).

It is interesting to note that the effect of pyridine is stronger in the case of Et-FIOH, as can be seen by a more drastic decrease in the cathodic current at $+0.95$ V as a function of pyridine concentration (Figure 6c). These results suggest the possibility that the proton removal from $\text{Et-FIOH}^{+\cdot}$ in the presence of pyridine occurs from either the $-\text{OH}$ or the $>\text{N}-\text{CH}_2-$ group, whereas the proton removal from Et-FIOMe occurs only from the $>\text{N}-\text{CH}_2-$ group. To investigate the acidities of $-\text{OH}$ and $>\text{N}-\text{CH}_2-$ protons in $\text{Et-FIOH}^{+\cdot}$, we optimized the $\text{Et-FIOH}^{+\cdot}$ structure using the DFT/B3LYP method and calculated the atomic charges using NPA analysis. The computed NPA charge densities indicated that the hydroxyl H-atom is the most positively charged H-atom in the molecule with a positive charge of 0.514, whereas the H-atoms on the two $>\text{N}-\text{CH}_2-$ groups carry the charge density of 0.230. These results suggest that the acidic proton is localized on the $-\text{OH}$ group of $\text{Et-FIOH}^{+\cdot}$. To understand the effect of pyridine in the cyclic voltammetry of Et-FIOH, we computed the thermochemistry of the two reactions: (a) $\text{Et-FIOH}^{+\cdot} + \text{PYR} \rightarrow \text{Et}(-\text{H}^+)\text{FIOH}\cdot + \text{PYRH}^+$ and (b) $\text{Et-FIOH}^{+\cdot} + \text{PYR} \rightarrow \text{EtFIO}\cdot + \text{PYRH}^+$. In the gas phase, both of the reactions are endothermic by 24 kcal/mol at the B3LYP/6-311++G**//B3LYP/6-31G* level of theory. However, when these two sets of calculations were carried using the PCM model (implicit solvation) of acetonitrile, both reactions became exothermic by 24 kcal/mol at the same level of theory. Therefore, the removal of proton from $\text{Et-FIOH}^{+\cdot}$ can occur from either the $-\text{OH}$ or the $>\text{N}-\text{CH}_2-$ moiety. In the following text, we will consider only the removal from the $>\text{N}-\text{CH}_2-$ group because this reaction explains the formation of electrochemically active products with reduction potentials at -0.20 and -1.0 V. (See the further text.)

So far, we have demonstrated that the one-electron oxidized Et-FIOH becomes acidic enough to lose protons in the presence of pyridine. In the absence of pyridine ($\text{p}K_{\text{a}}$ of pyridinium ion is 5.2),⁶⁵ neutral Et-FIOH ($\text{p}K_{\text{a}}$ of the pseudobase is 3.6) can serve as a base. Because Et-FIOH is a weaker base, it cannot remove protons from one-electron oxidized $\text{Et-FIOH}^{+\cdot}$ radical cation, as demonstrated by reversible one-electron oxidation peak in Figure 1b. However, Et-FIOH could abstract protons from more acidic Et-FIOH^{2+} , which would explain the appearance of Et-FI^+ during anodic oxidation of Et-FIOH. If this was the case, then the two-electron oxidation of Et-FIOH in the absence of pyridine would give rise to the same products as

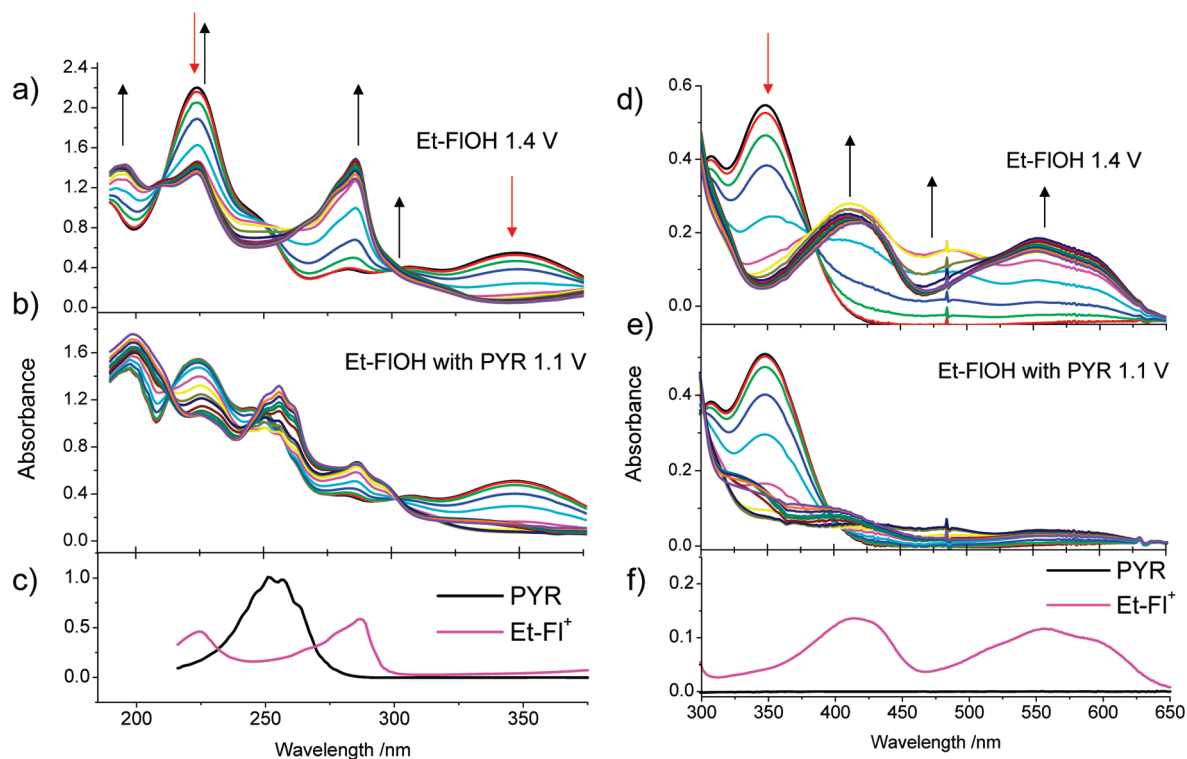


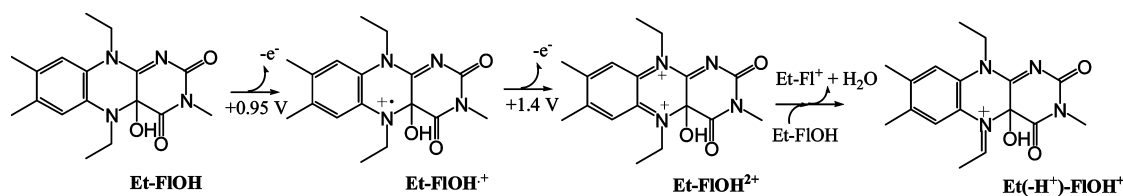
Figure 8. (a,d) UV/vis absorption spectral changes during the controlled potential electrolysis of Et-FIOH (3 mM) in acetonitrile at +1.4 V. (b,e) Controlled potential electrolysis at +1.1 V of Et-FIOH (3 mM in acetonitrile) in the presence of 5 mM pyridine. The spectra in parts a, b, d, and e were collected at the following time intervals: 0, 2, 10, 20, 30, 40, 50, 60, 70, 90, 120, 180, 240, 300, 420, and 600 s. (c,f) Absorption spectra of pyridine and Et-FI⁺.

one-electron oxidation of Et-FIOH in the presence of pyridine. The following experiments are aimed at comparing the two processes.

Figure 7a demonstrates that one-electron oxidation of Et-FIOMe leads to the appearance of two additional peaks in the cathodic scan: at -0.2 and -1.0 V. The same results were obtained in the case of Et-FIOH (data not shown). We assign the two peaks to decomposition products obtained from iminium ion, Et($-H^+$)-FIOH⁺. It is interesting to note that the same two reduction peaks were obtained in variable scan-rate cyclic voltammograms of Et-FIOH in the absence of pyridine. Whereas we did not observe these peaks at 0.1 V/s scan rates, an increase in the scan rate from 0.1 to 25 V/s lead to the growth of peaks at -0.2 and -1.0 V. These results strongly suggest that the two-electron oxidation of Et-FIOH in the absence of pyridine leads to the same intermediates as one-electron oxidation of Et-FIOH/Et-FIOMe in the presence of pyridine. On the basis of these results, we propose the mechanism for Et-FI⁺ formation during anodic oxidation of Et-FIOH in Scheme 2. One-electron oxidation of Et-FIOH at +0.95 V forms Et-FIOH^{•+} radical cation, which is stable in the absence of pyridine. Subsequent one-electron oxidation at $\sim +1.4$ V creates a dication, Et-FIOH²⁺, which loses a proton to produce iminium ion Et($-H^+$)-FIOH⁺. The base responsible for proton abstraction is Et-FIOH, which leads to the formation of Et-FI⁺ and water.

The further decomposition of iminium ion Et($-H^+$)-FIOH⁺ is not clear. One possible pathway involves the cleavage of N-alkyl chain to produce methyl-lumiflavin (Me-Lf) and acetaldehyde. Me-Lf exhibits one-electron reduction peak at -1.0 V,⁶⁶ which coincides with the peak we observe upon two-electron oxidation of Et-FIOH. To investigate this mechanism, we performed UV/vis spectroelectrochemical measurements on Et-FIOH, and we found no evidence of Me-Lf formation, which exhibits strong absorption at 443 nm⁶⁶ (Figure 8). The UV/vis

spectra were obtained for two samples: (i) Et-FIOH in the presence of pyridine using +1.1 V of applied voltage and (ii) Et-FIOH in the absence of pyridine using a potential of +1.4 V. In the absence of pyridine, the disappearance of 350 nm absorption band that corresponds to Et-FIOH is concurrent with the growth of three absorption peaks in the visible range at 414, 485, and 554 nm (Figure 8d). The peak at 485 nm grows during the initial 45 s but disappears at longer times and is assigned to the absorption of Et-FIOH^{•+}.²⁰ The bands at 414 and 554 nm are assigned to Et-FI⁺, whose visible absorption spectrum is shown in Figure 8f. The presence of Et-FIOH^{•+} and Et-FI⁺ absorption bands is consistent with the mechanism proposed in the Scheme 2. The absorption band corresponding to Me-Lf at 443 nm was not observed, suggesting a different decomposition pathway for Et($-H^+$)-FIOH⁺ iminium ion. Because no additional bands were observed in the visible range, we conclude that the product of Et($-H^+$)-FIOH⁺ decomposition does not absorb in the visible range. Figure 8a shows the changes that occur in the UV range during electrolysis of Et-FIOH solution at +1.4 V. After 10 min of electrolysis, the absorption band of Et-FIOH at 350 nm fully disappears, and four new absorption bands appear at 300, 286, 222, and 194 nm. Absorption bands at 222 and 286 nm partially originate from Et-FI⁺, whereas the rest of the absorption bands are assigned to the absorption of the product(s) of Et($-H^+$)-FIOH⁺ decomposition. The fact that the product absorbs in the UV region (below 300 nm) suggests that the decomposition of Et($-H^+$)-FIOH⁺ does not lead to the Me-Lf formation but possibly to the cleavage of the isoalloxazine ring. Figure 8b,e shows the spectral changes during +1.1 V electrolysis of Et-FIOH in the presence of pyridine. In this case, the absorption bands from Et-FI⁺ at 222, 286, 414, and 554 nm are much weaker. This is consistent with the fact that in the presence of pyridine Et-FIOH does not abstract protons from oxidized Et-FIOH to produce Et-FI⁺ and water. After 10 min

SCHEME 2: Proposed Mechanism for the Release of Et-FI⁺ during Anodic Oxidation of Et-FIOH

of electrolysis, the spectrum consists of weak absorption bands due to Et-FI⁺ and additional bands at 184, 256, and 300 nm. The band at 256 nm appears in the same spectral range as the pyridine absorption (Figure 8c), and it might arise because of the absorption of pyridinium ion formed during PCET. Again, the rest of the absorption bands are assigned to the absorption of Et(-H⁺)-FIOH⁺ decomposition products. It is interesting to note that the absorption spectrum obtained upon chemical oxidation of Et-FIOH with persulfate ions exhibits absorption at 300 nm (Figure 5), possibly due to same oxidation products. Therefore, we conclude that the decomposition of Et(-H⁺)-FIOH⁺ gives rise to the product with longest the wavelength absorption at 300 nm, suggesting a cleavage of the isoalloxazine ring.

Given the results presented in this manuscript, we conclude that the production of Et-FI⁺ during the anodic oxidation of Et-FIOH does not involve the formation of OH⁺, as previously hypothesized.²⁰ Instead, we propose that the formation of Et-FI⁺ occurs via a shift in the Et-FIOH/Et-FI⁺ acid–base equilibrium due to the formation of a strong Bronsted acid, Et-FIOH²⁺. Because this pathway does not lead to catalytic water oxidation, we are currently developing pseudobase model compounds that lack α H-atoms on the N-alkyl chain.

Conclusions

This article describes the oxidation behavior of Et-FIOH, a flavin-based pseudobase derived from N(5)-ethyl-flavinium perchlorate (Et-FI⁺). Previous experiments involving cyclic voltammetry of Et-FIOH²⁰ suggested that the two-electron oxidation of Et-FIOH produces a dication Et-FIOH²⁺ that releases hydroxyl cation and Et-FI⁺. Because such a reaction could lead to the development of a purely organic water oxidation catalyst, we investigated the process in more detail. Our findings suggest that the release of hydroxyl cation does not occur in the electrochemistry of Et-FIOH. Instead, we find that the production of Et-FI⁺ is associated with the shift in the Et-FIOH/Et-FI⁺ acid–base equilibrium due to the formation of Bronsted and Lewis acids during anodic oxidation of Et-FIOH. We present several experiments that support this assignment: (i) We electrolyzed the electrolyte solution (0.1 M TBAP in acetonitrile) at +2 V, after which we added Et-FIOH to the solution. We observed the production of Et-FI⁺ even though Et-FIOH was not oxidized. The amount of generated Et-FI⁺ correlated with the amount of water present in the acetonitrile solution. These results suggest that the anodic oxidation of water leads to a pH decrease in the electrolyte solution, which in turn leads to the conversion of Et-FIOH to Et-FI⁺. (ii) We investigated the reactions between Et-FIOH and a series of chemical oxidants and found that the formation of Et-FI⁺ does not correlate with the oxidizing power of the reagent used. Instead, the formation of Et-FI⁺ correlates with Lewis acidities of oxidizing agents used in the study. (iii) The anodic oxidation of Et-FIOH in the presence of pyridine as a base demonstrates that the PCET from Et-FIOH radical cation occurs. The proton loss occurs from the N(5)-CH₂ moiety of the molecule, as

demonstrated by oxidation experiments involving Et-FIOME derivative. However, DFT calculations suggest that the proton loss in Et-FIOH⁺ can occur from either >N-CH₂- or -OH moiety of the molecule. Upon PCET in Et-FIOH and Et-FIOME, two additional reduction peaks were observed at -0.2 and -1.0 V. The same products were observed upon the two-electron oxidation of Et-FIOH, suggesting that Et-FIOH²⁺ releases protons in the absence of pyridine. The released protons then shift the Et-FIOH/Et-FI⁺ equilibrium, giving rise to the formation of Et-FI⁺ reduction peaks observed in the cyclic voltammetry of Et-FIOH.

These findings provide valuable information for studies of possible catalytic water oxidation by pseudobase derivatives. We identified that the loss of a proton from N(5) alkyl chain leads to the decomposition of the flavin pseudobase via an iminium ion formation. For a design of a catalytic system, this process needs to be deactivated by a preparation of pseudobases that lack α H-atoms at the N(5) R group.

Acknowledgment. Spectroelectrochemical and bulk electrolysis experiments were conducted using the equipment provided by Dr. Felix N. Castellano (Bowling Green State University). K.D.G. thanks Drs. Felix N. Castellano (Bowling Green State University) and Amar H. Flood (Indiana University) for useful discussions. K.D.G. thanks Bioanalytical Systems for their donation of the carbon electrode for bulk electrolysis. C.M.H. thanks the Ohio Supercomputer Center and the NSF for computational and financial support.

Supporting Information Available: Discussion of possible water oxidation catalysis by Et-FIOH and accompanying DFT calculations. This material is available free of charge via the Internet at <http://pubs.acs.org>.

References and Notes

- (1) Van Berkel, W. J. H.; Kamerbeek, N. M.; Fraaije, M. W. *J. Biotechnol.* **2006**, *124*, 670–689.
- (2) Meighen, E. A.; Dunlap, P. V. *Physiological, Biochemical and Genetic-Control of Bacterial Bioluminescence*. In *Advances in Microbial Physiology*; Academic Press: London, 1993; pp 1–67.
- (3) Imada, Y.; Kitagawa, T.; Ohno, T.; Iida, H.; Naota, T. *Org. Lett.* **2010**, *12*, 32–35.
- (4) Kemal, C.; Chan, T. W.; Bruice, T. C. *Proc. Natl. Acad. Sci. U.S.A.* **1977**, *74*, 405–409.
- (5) Imada, Y.; Iida, H.; Naota, T. *J. Am. Chem. Soc.* **2005**, *127*, 14544–14545.
- (6) Murahashi, S.; Oda, T.; Masui, Y. *J. Am. Chem. Soc.* **1989**, *111*, 5002–5003.
- (7) Ball, S.; Bruice, T. C. *J. Am. Chem. Soc.* **1979**, *101*, 4017–4019.
- (8) Minidis, A. B. E.; Backvall, J. E. *Chem.—Eur. J.* **2001**, *7*, 297–302.
- (9) Linden, A. A.; Kruger, L.; Backvall, J. E. *J. Org. Chem.* **2003**, *68*, 5890–5896.
- (10) Bruice, T. C. *J. Chem. Soc., Chem. Commun.* **1983**, 14–15.
- (11) Mager, H. I. X.; Tu, S. C. *Tetrahedron* **1994**, *50*, 6759–6766.
- (12) Imada, Y.; Iida, H.; Murahashi, S. I.; Naota, T. *Angew. Chem., Int. Ed.* **2005**, *44*, 1704–1706.
- (13) Mazzini, C.; Lebreton, J.; Furstoss, R. *J. Org. Chem.* **1996**, *61*, 8–9.

- (14) Murahashi, S. I.; Ono, S.; Imada, Y. *Angew. Chem., Int. Ed.* **2002**, *41*, 2366–2368.
- (15) Gelalcha, F. G. *Chem. Rev.* **2007**, *107*, 3338–3361.
- (16) Imada, Y.; Iida, H.; Ono, S.; Murahashi, S. I. *J. Am. Chem. Soc.* **2003**, *125*, 2868–2869.
- (17) Kemal, C.; Bruce, T. C. *Proc. Nat. Acad. Sci. U.S.A.* **1976**, *73*, 995–999.
- (18) Lei, B. F.; Ding, Q. Z.; Tu, S. C. *Biochemistry* **2004**, *43*, 15975–15982.
- (19) Merenyi, G.; Lind, J. *J. Am. Chem. Soc.* **1991**, *113*, 3146–3153.
- (20) Mager, H. I. X.; Sazou, D.; Liu, Y. H.; Tu, S. C.; Kadish, K. M. *J. Am. Chem. Soc.* **1988**, *110*, 3759–3762.
- (21) Eberlein, G.; Bruce, T. C. *J. Am. Chem. Soc.* **1983**, *105*, 6685–6697.
- (22) Muto, S.; Bruce, T. C. *J. Am. Chem. Soc.* **1982**, *104*, 2284–2290.
- (23) Ghisla, S.; Hartmann, U.; Hemmeric, P.; Muller, F. *Justus Liebig's Ann. Chem.* **1973**, 1388–1415.
- (24) Ruttinger, W.; Dismukes, G. C. *Chem. Rev.* **1997**, *97*, 1–24.
- (25) Gersten, S. W.; Samuels, G. J.; Meyer, T. J. *J. Am. Chem. Soc.* **1982**, *104*, 4029–4030.
- (26) McDaniel, N. D.; Coughlin, F. J.; Tinker, L. L.; Bernhard, S. *J. Am. Chem. Soc.* **2008**, *130*, 210–217.
- (27) Rotzinger, F. P.; Munavalli, S.; Comte, P.; Hurst, J. K.; Graetzel, M.; Pern, F. J.; Frank, A. J. *J. Am. Chem. Soc.* **1987**, *109*, 6619–6626.
- (28) Zong, R.; Thummel, R. P. *J. Am. Chem. Soc.* **2005**, *127*, 12802–12803.
- (29) Kohl, S. W.; Weiner, L.; Schwartsburd, L.; Konstantinovskii, L.; Shimon, L. J. W.; Ben-David, Y.; Iron, M. A.; Milstein, D. *Science* **2009**, *324*, 74–77.
- (30) Cape, J. L.; Hurst, J. K. *J. Am. Chem. Soc.* **2008**, *130*, 827–829.
- (31) Kanan, M. W.; Nocera, D. G. *Science* **2008**, *321*, 1072–1075.
- (32) Limburg, J.; Vrettos, J. S.; Liable-Sands, L. M.; Rheingold, A. L.; Crabtree, R. H.; Brudvig, G. W. *Science* **1999**, *283*, 1524–1527.
- (33) Brown, S. A.; Rizzo, C. J. *Synth. Commun.* **1996**, *26*, 4065–4080.
- (34) Epple, R.; Wallenborn, E.-U.; Carell, T. *J. Am. Chem. Soc.* **1997**, *119*, 7440–7451.
- (35) Tracy, M.; Acton, E. M. *J. Org. Chem.* **1984**, *49*, 5116–5124.
- (36) Kuhn, R.; Weygand, F. *Ber. Dtsch. Chem. Ges. B* **1934**, *67B*, 1409–1413.
- (37) Mager, H. I. X.; Addink, R. *Tetrahedron* **1985**, *41*, 183–190.
- (38) Hua, F.; Kinayyigit, S.; Rachford, A. A.; Shikhova, E. A.; Goeb, S.; Cable, J. R.; Adams, C. J.; Kirschbaum, K.; Pinkerton, A. A.; Castellano, F. N. *Inorg. Chem.* **2007**, *46*, 8771–8783.
- (39) Frisch, M. J.; Trucks, G. W.; Schlegel, H. B.; Scuseria, G. E.; Robb, M. A.; Cheeseman, J. R.; Montgomery, J. A., Jr.; Vreven, T.; Kudin, K. N.; Burant, J. C.; Millam, J. M.; Iyengar, S. S.; Tomasi, J.; Barone, V.; Mennucci, B.; Cossi, M.; Scalmani, G.; Rega, N.; Petersson, G. A.; Nakatsuji, H.; Hada, M.; Ehara, M.; Toyota, K.; Fukuda, R.; Hasegawa, J.; Ishida, M.; Nakajima, T.; Honda, Y.; Kitao, O.; Nakai, H.; Klene, M.; Li, X.; Knox, J. E.; Hratchian, H. P.; Cross, J. B.; Bakken, V.; Adamo, C.; Jaramillo, J.; Gomperts, R.; Stratmann, R. E.; Yazyev, O.; Austin, A. J.; Cammi, R.; Pomelli, C.; Ochterski, J. W.; Ayala, P. Y.; Morokuma, K.; Voth, G. A.; Salvador, P.; Dannenberg, J. J.; Zakrzewski, V. G.; Dapprich, S.; Daniels, A. D.; Strain, M. C.; Farkas, O.; Malick, D. K.; Rabuck, A. D.; Raghavachari, K.; Foresman, J. B.; Ortiz, J. V.; Cui, Q.; Baboul, A. G.; Clifford, S.; Cioslowski, J.; Stefanov, B. B.; Liu, G.; Liashenko, A.; Piskorz, P.; Komaromi, I.; Martin, R. L.; Fox, D. J.; Keith, T.; Al-Laham, M. A.; Peng, C. Y.; Nanayakkara, A.; Challacombe, M.; Gill, P. M. W.; Johnson, B.; Chen, W.; Wong, M. W.; Gonzalez, C.; Pople, J. A. *Gaussian 03*, revision C.02; Gaussian, Inc.: Wallingford, CT, 2004.
- (40) Lee, C. T.; Yang, W. T.; Parr, R. G. *Phys. Rev. B* **1988**, *37*, 785–789.
- (41) Becke, A. D. *J. Chem. Phys.* **1993**, *98*, 5648–5652.
- (42) Tomasi, J.; Persico, M. *Chem. Rev.* **1994**, *94*, 2027–2094.
- (43) Cossi, M.; Barone, V.; Cammi, R.; Tomasi, J. *Chem. Phys. Lett.* **1996**, *255*, 327–335.
- (44) Barone, V.; Cossi, M.; Tomasi, J. *J. Chem. Phys.* **1997**, *107*, 3210–3221.
- (45) Cossi, M.; Barone, V. *J. Chem. Phys.* **1998**, *109*, 6246–6254.
- (46) Barone, V.; Cossi, M.; Tomasi, J. *J. Comput. Chem.* **1998**, *19*, 404–417.
- (47) Cramer, C. J.; Truhlar, D. G. *Chem. Rev.* **1999**, *99*, 2161–2200.
- (48) Park, M. Y.; Yang, S. G.; Jadhav, V.; Kim, Y. H. *Tetrahedron Lett.* **2004**, *45*, 4887–4890.
- (49) Ebersson, L.; Schäfer, H. *Organic Electrochemistry*. In *Organic Electrochemistry*; Springer-Verlag: New York, 1971; p 26.
- (50) Maki, A. H.; Geske, D. H. *J. Chem. Phys.* **1959**, *30*, 1356–1357.
- (51) Zhang, Y.; Flowers, R. A. *J. Org. Chem.* **2003**, *68*, 4560–4562.
- (52) Lee, K. Y.; Kuchynka, D. J.; Kochi, J. K. *Inorg. Chem.* **1990**, *29*, 4196–4204.
- (53) Zuo, Z. H.; Katsumura, Y.; Ueda, K.; Ishigure, K. *J. Chem. Soc., Faraday Trans.* **1997**, *93*, 533–536.
- (54) Kaljurand, I.; Kutt, A.; Soovali, L.; Rodima, T.; Maemets, V.; Leito, I.; Koppel, I. A. *J. Org. Chem.* **2005**, *70*, 1019–1028.
- (55) Costentin, C. *Chem. Rev.* **2008**, *108*, 2145–2179.
- (56) Cukier, R. I.; Nocera, D. G. *Annu. Rev. Phys. Chem.* **1998**, *49*, 337–369.
- (57) Huynh, M. H. V.; Meyer, T. J. *Chem. Rev.* **2007**, *107*, 5004–5064.
- (58) Merenyi, G.; Lind, J.; Mager, H. I. X.; Tu, S. C. *J. Phys. Chem.* **1992**, *96*, 10528–10533.
- (59) Mayer, J. M.; Rhile, I. J. *Biochim. Biophys. Acta* **2004**, *1655*, 51–58.
- (60) Greaves, M. D.; Niemz, A.; Rotello, V. M. *J. Am. Chem. Soc.* **1999**, *121*, 266–267.
- (61) Gupta, N.; Linschitz, H. *J. Am. Chem. Soc.* **1997**, *119*, 6384–6391.
- (62) Amatore, C.; Capobianco, G.; Farnia, G.; Sandona, G.; Saveant, J. M.; Severin, M. G.; Vianello, E. *J. Am. Chem. Soc.* **1985**, *107*, 1815–1824.
- (63) Baciocchi, E.; Lapi, A. *Tetrahedron Lett.* **1999**, *40*, 5425–5428.
- (64) Steenken, S.; Vieira, A. *Angew. Chem., Int. Ed.* **2001**, *40*, 571–573.
- (65) Serjeant, E. P.; Dempsey, B. *Ionisation Constants of Organic Acids in Solution*; Serjeant, E. P., Dempsey, B., Eds.; IUPAC Chemical Data Series No. 23; Pergamon Press: Oxford, U.K., 1979.
- (66) Niemz, A.; Imbriglio, J.; Rotello, V. M. *J. Am. Chem. Soc.* **1997**, *119*, 887–892.
- (67) Bosch, E.; Roses, M. *Anal. Chem.* **1988**, *60*, 2008–2013.
- (68) Hardwick, T. J.; Robertson, E. *Can. J. Chem.* **1951**, *29*, 818–827.
- (69) Ridd, J. H. *Adv. Phys. Org. Chem.* **1978**, *16*, 1–49.
- (70) Huang, K. C.; Couttenye, R. A.; Hoag, G. E. *Chemosphere* **2002**, *49*, 413–420.

JP104443Y